Reaction mechanisms in the system ^{20}Ne + ^{165}Ho: Measurement and analysis of forward recoil range distributions

D. Singh,[1] R. Ali,[1] M. Afzal Ansari,[1,*] M. H. Rashid,[2] R. Guin,[2] and S. K. Das[2]
[1]*Department of Physics, Aligarh Muslim University, Aligarh-202002, India*
[2]*Variable Energy Cyclotron Centre, 1/AF Bidhan Nagar, Kolkata-700064, India*
(Received 4 December 2007; revised manuscript received 17 January 2009; published 4 May 2009)

Keeping in view the study of complete and incomplete fusion of heavy ions with a target, the forward recoil range distributions of several evaporation residues produced at 164 MeV ^{20}Ne-ion beam energy have been measured for the system ^{20}Ne + ^{165}Ho. The recoil catcher activation technique followed by off-line gamma spectroscopy has been employed. Measured forward recoil range distributions of these evaporation residues show evidence of several incomplete fusion channels in addition to complete fusion. The entire and partial linear momentum transfers inferred from these recoil range distributions were used to identify the evaporation residues formed by complete and incomplete fusion mechanisms. The results indicate the occurrence of incomplete fusion involving the breakup of ^{20}Ne into ^{4}He + ^{16}O and/or ^{8}Be + ^{12}C followed by fusion of one of the fragments with target nucleus ^{165}Ho. Complete and incomplete fusion reaction channels have been identified in the production of various evaporation residues and an attempt has been made to separate out relative contributions of complete and incomplete fusion components from the analysis of the measured recoil range distribution data. The total contribution of complete and incomplete fusion channels has also been estimated.

DOI: 10.1103/PhysRevC.79.054601 PACS number(s): 25.70.Gh, 25.70.Jj

I. INTRODUCTION

The study of heavy ion (HI) fusion reactions above the Coulomb barrier has been the subject of interest in nuclear physics for the past few decades. Moreover, in recent years there has been a renewed interest in the study of incomplete fusion reactions in heavy ion interactions at energies below 10 MeV/nucleon [1–7]. In the interaction of two heavy ions a number of reaction channels open and a transfer of clusters of nucleons and angular momentum takes place. Nuclei produced in heavy ion (HI) fusion reactions are characterized by excitation energy and angular momentum and their decay is governed by both these quantities. The most dominant reaction process above the Coulomb barrier is the formation and decay of the equilibrated compound nucleus following the entire projectile fusion with the target nucleus which is termed as complete fusion (CF). As the projectile energy increases above the Coulomb barrier, compound nucleus formation is hindered and incomplete fusion (ICF) starts competing with complete fusion (CF). In the ICF reaction process, which is characterized by the fractional fusion of the projectile, the projectile is assumed to break up into the fragments (e.g., ^{20}Ne-ion may break up into ^{16}O + α-particle and /or ^{8}Be + ^{12}C) and one of the fragments fuses with the target nucleus while remaining part moves in the forward direction [8–10]. The excited composite system formed as a result of the fusion of the fragment of the incident ion with the target may also undergo deexcitation by emission of particles and/or γ-rays.

The possibilities of ICF were first pointed by Britt and Quinton [11], who observed the breakup of the incident projectiles like ^{12}C, ^{14}N, and ^{16}O into alpha clusters in an interaction with the surface of the target nucleus at ≈10.5 MeV/nucleon energy. However, major advances in the study of ICF reactions took place after the work of Inamura *et al.* [12] for the ^{14}N + ^{159}Tb system at a beam energy of ≈7 MeV/nucleon, wherein exclusive measurements of forward-peaked alpha-particles in coincidence with the prompt gamma-rays of evaporation residues produced were carried out. Measurement of recoil range distributions (RRD) of evaporation residues [1–7], using the activation technique [13] in heavy ion reactions below 10 MeV/nucleon, has further supported the occurrence of the ICF process. It is worthwhile to mention that most of the studies on ICF at lower beam energies have been carried out with projectiles like ^{12}C and ^{16}O near and above the Coulomb barrier. However, such types of studies using a ^{20}Ne-ion beam as a projectile with heavy targets below 10 MeV/nucleon are scarce. More experimental data on recoil range distributions (RRDs) of the evaporation residues (ERs) are demanded to have better insight into heavy ion (HI) reaction mechanisms that are involved at energies above the Coulomb barrier and below 10 MeV/nucleon. Special interest lies in the understanding of degrees of linear momentum transfer in the interaction of a HI projectile with the target. It is possible to separate out the relative contributions of various ICF channels from the measurement of RRDs of ERs at a given projectile energy. The observed RRDs of the produced heavy residues depend on the linear momentum transferred in the reaction. In the CF process, the linear momentum of the projectile is completely transferred to the target nucleus. Thus, the compound system carries the entire linear momentum and hence recoils a large distance in the stopping medium. However, in the ICF process partial or incomplete transfer of linear momentum takes place and the composite system produced in such a process recoils a smaller distance in the stopping medium. Measurement of recoil range can also be

*drmafzalansari@yahoo.com

used to distinguish different ICF processes where the same residue may be formed by fusion of different fragments in the projectile breakup with the target, followed by different groups of particle emission. The RRDs of the ERs measured by the recoil catcher technique and γ-ray spectroscopy provide direct evidence of linear momentum transfer from projectile to target nucleus.

Several models have been proposed to explain ICF reactions. The sum rule model of Wilczynski *et al.* [14] assumes that the various ICF channels are localized in the angular momentum space above the critical angular momentum for the complete fusion of the projectile and target. The break-up fusion (BUF) model of Udagawa and Tamura [15] based on a DWBA formalism explained ICF in terms of a breakup of the projectile in the nuclear field (e.g., projectile ^{20}Ne may break up into $^{16}O + {}^{4}He$ and/or $^{12}C + {}^{8}Be$) as it approaches the nuclear field of the target nucleus. It is assumed that either of the fragments may fuse with the target nucleus, while the remnant moves as a spectator and gives rise to the projectile like fragments (PLFs). Other models include the hot spot model [16], promptly emitted particle (PEP) model [17], and multistep direct reaction model [18]. The existing models have been used to fit the experimental data above 10.5 MeV/nucleon energies. However, at energies less than 10 MeV/nucleon, no theoretical model is available to explain ICF process data satisfactorily.

Most of the earlier ICF studies have been confined to low Z-projectile ($Z \leqslant 10$), induced reactions on targets of medium mass ($A \leqslant 100$). There have been very few studies with heavier targets ($A > 150$). In the case of low and medium mass target nuclei, the ICF cross section is a small fraction of the total cross section of the evaporation residues (ERs). However, in case of heavier target nuclei, the evaporation of alpha particle(s) from the compound nucleus (CN) becomes less probable because of the high Coulomb barrier. Consequently, the emission of a single or clusters of alpha particles are mostly associated with ICF process observed in the breakup of the projectile. In order to have a better understanding of the underlying processes a comprehensive study of the excitation function and recoil range distribution of evaporation residues produced in HI induced reactions has been undertaken by our group, as a part of ongoing program to study CF and ICF in heavy ion induced reactions [19–21]. In the present work the recoil range distributions (RRDs) of evaporation residues produced at 164 MeV ^{20}Ne-ion beam have been measured. The present measurements of the recoil range distribution of the residues produced via alpha particles emission channels (produced in the breakup of the projectile) generally show major contributions from the ICF process. An attempt has also been made to separate out relative contributions of complete fusion and incomplete fusion components from the analysis of measured RRD data. To the best of our knowledge RRDs for the above system have been measured for the first time. It is worth mentioning that some of the long-lived residues may have contributions from the decay of higher charge short-lived precursor isobars in the observed γ-ray intensities hence the measured ICF fraction may have some uncertainty, but will not affect the relative ICF/CF contributions in the individual residue. However, in the present work the emphasis is given to the understanding of the breakup of the projectile leading to on ICF process and not to the absolute cross-section values.

II. EXPERIMENTAL DETAILS

The experiments have been carried out using the heavy ion accelerator facility of the Variable Energy Cyclotron Centre (VECC), Kolkata, India. The thin foil catcher technique has been employed [9]. Forward recoil range distributions (RRDs) for a number of radioactive evaporation residues produced in the reactions of ^{20}Ne on ^{165}Ho, recoiling into thin aluminium catcher foils were measured at 164 MeV ^{20}Ne ion beam. For the measurement of RRDs, a thin holmium target foil backed by a stack of thin aluminium catcher foils was used. Details of target preparation, target-catcher irradiation, post irradiation analysis including energy and efficiency calibrations, etc., are given in the following sections.

A. Target preparation and irradiation

A self-supporting natural ^{165}Ho target with a purity better than 99.9% was prepared by rolling machine of the desired thickness at Saha Institute of Nuclear Physics (SINP) Target Lab, Kolkata, India. The thin Al-catcher foils of a thickness lying between 76–100 μg/cm^2 were prepared by using the vacuum evaporation technique, at VECC Target Lab. The thickness of each target foil was determined using microbalance as well as by the α-particle transmission method, which is based on the measurement of the energy loss by 5.485 MeV α-particles obtained from the ^{241}Am source, while passing through the target. The thickness of the holmium target foil was found to be $\approx$465 μg/cm^2. The target was cut into a size of 1.5×1.5 cm^2 and was pasted on a rectangular aluminium target holder having a concentric hole of 1.2 cm diameter. The aluminium target holder was used for rapid heat dissipation. A stack of 15 thin Al-catcher foils was kept behind a ^{165}Ho target to trap at various aluminum thicknesses, the recoiled residues produced via CF and ICF processes. The target-catchers assembly was bombarded with 164 MeV ^{20}Ne ion beams in a specially designed vacuum chamber at Variable Energy Cyclotron Centre (VECC), Kolkata, India. A schematic diagram of the experimental setup used for target irradiation is shown in Fig. 1. The weighted average beam current of $\approx$40 nA was measured behind the target assembly with an electron suppressed Faraday cup, using a current integrator device. Keeping in view the half-lives of interest, irradiations have been carried out for about 9 h duration. The beam fluxes measured by two methods (time weighted beam current and total charge collected in Faraday cup) were found to agree with each other within a 10% variation. The mean energy of the ^{20}Ne ion beam incident at half the thickness on each foil in the stack was calculated from the energy degradation of the incident beam energy, using stopping power and range software SRIM [22]. The inherent energy spread in 164 MeV ^{20}Ne beam is reported as 500 keV. When the beam passes through the target, the energy spread due to straggling may come into picture. However, the energy spread due to straggling has not been considered due to its insignificant contribution [23].

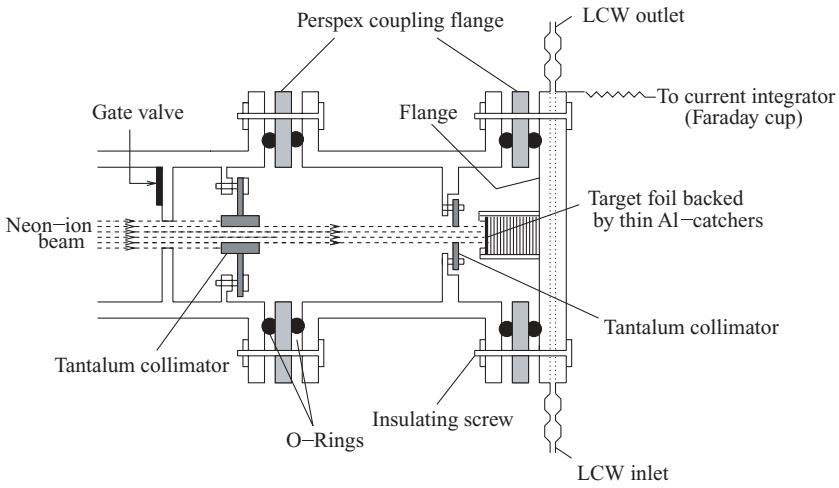

FIG. 1. The experimental setup used for target-catchers irradiation.

B. Post-irradiation analysis

After the irradiation, a stack of aluminium catchers backed by target foil was taken out of the irradiation chamber and each catcher foil was counted separately for γ-ray activities of evaporation residues (ERs) using a 60 cc HPGe detector, coupled to a PC based data acquisition system. The γ-ray spectrum of each foil has been recorded at increasing times so that the decay curve analysis can be done to measure the half-lives of the residues. Software MAESTRO [24] and FREEDOM [25] have been used for recording and analysis of the nuclear data, respectively. The energy calibration of the detector was done using ^{152}Eu γ-ray source. The resolution of the HPGe detector was found to be 1.9 keV at 1.33 MeV γ-rays of ^{60}Co. The geometry dependent photopeak detection efficiencies of the HPGe detector at various source-detector distances were measured using ^{152}Eu γ-ray source of known strength. The source-detector distance was adjusted for the counting of the irradiated sample so that dead time of the detector was always less than 10%. Moreover, the counting was carried out in live-time mode of the multichannel analyzer to incorporate the dead time loss. The γ-rays intensities have been used to calculate the experimentally measured cross sections corresponding to the various ERs. A typical γ-ray spectrum of an Al-catcher foil obtained after irradiation of ^{165}Ho foil by 164 MeV ^{20}Ne-ion beam is shown in Fig. 2. The ERs were identified by their characteristic γ-rays. Measured half-lives of the evaporation residues are found to be in good agreement with the literature values. The characteristic γ-rays energies, half-lives of residual nuclei, branching ratio of the γ-rays, abundance, etc., are taken from the Table of Isotopes [26].

The cross sections $\sigma_r(E)$ for a particular reaction product in different catcher foils were determined using the expression [27]:

$$\sigma_r(E) = \frac{A\lambda \exp(\lambda t_2)}{N_0 \phi \vartheta \varepsilon_G K [1 - \exp(-\lambda t_1)[1 - \exp(-\lambda t_3)]}, \quad (1)$$

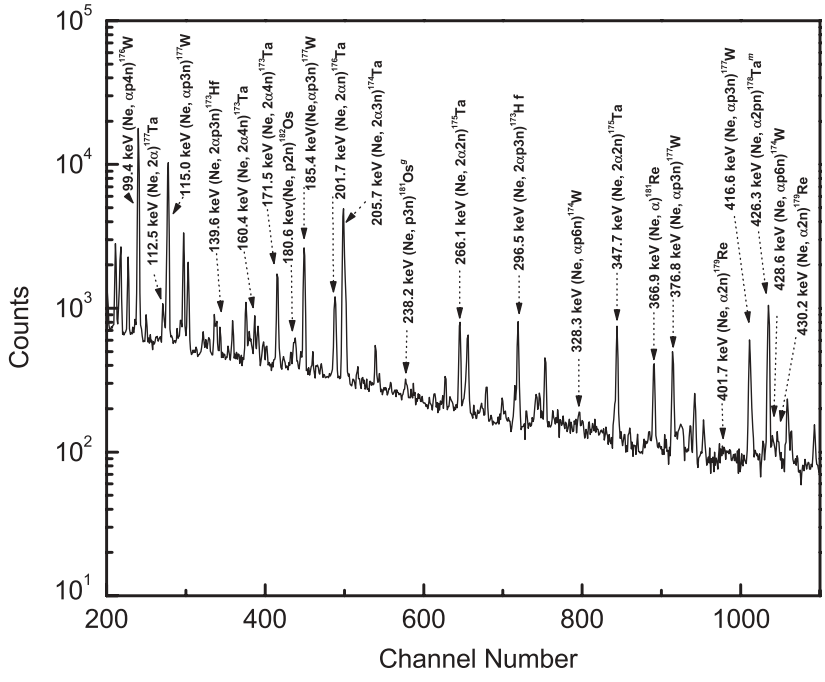

FIG. 2. Typical γ-ray energy spectrum of an aluminium catcher foil at cumulative thickness 637 μg/cm^2 obtained after irradiation of ^{165}Ho foil by ≈164 MeV ^{20}Ne-ion beam.

where A is the total number of counts observed under the photopeak of characteristic γ-ray in time t_3, λ is decay constant of the residual nucleus, N_0 is the total number of nuclei present in the target, ϕ is the incident ion beam flux, θ is the branching ratio of the identifying γ-ray, ε_G is the geometry dependent efficiency of the detector, t_1 is the irradiation time, t_2 is the time lapse between the end of irradiation and the start of counting and t_3 in the data collection time, $K = [1 - \exp(-\mu d)]/\mu d$ is the correction factor for self-absorption of the gamma-ray in the catcher foil with the absorption coefficient μ for the catcher of thickness 'd.' The factor $[1 - \exp(-\lambda t_1)]$ takes care of the decay of evaporation residue during irradiation time 't_1' and is known as the 'saturation correction factor.' The correction factor for the decay of the induced activity due to delay time 't_2' between the stop of irradiation and the start of counting is taken care of by $[\exp(-\lambda t_2)]$ and the correction factor due to the decay of the irradiated sample during data accumulation time 't_3' is taken as $[1 - \exp(-\lambda t_3)]$. The spectroscopic data used for yield calculations are listed in Table I. Recoil range distributions for 15 reactions have been measured at projectile energy ≈164 MeV and are listed in Table I. The measured recoil range distributions are plotted in Figs. 3(a)–3(f), 4(a)–4(f), and 5(a)–5(c). Details of error analysis and uncertainties in the measurements are given in our earlier Ref. [19]. It is important to mention that the higher Z short-lived precursors decay contributions may increase the observed γ-ray intensities that lead to enhancement in the absolute cross-section values in the production of some of the residues in the isobaric series. However, in the present work emphasis is given to the estimation of relative contributions ICF/CF in the individual residue which will not be affected.

TABLE I. List of reaction residues, the identifying γ-rays and their branching ratios.

Reactions	Half-life	E_γ (keV)	Branching ratio, θ (%)
^{165}Ho(Ne, $p2n$)^{182}Os	21.60 h	180.6[a]	34.7
^{165}Ho(Ne, $p3n$)^{181}Os^{g}	1.75 h	238.2[a]	44.0
		826.7	20.0
^{165}Ho(Ne,α)^{181}Re	19.90 h	366.9[a]	57.0
^{165}Ho(Ne,$\alpha 2n$)^{179}Re	19.70 min	430.2[a]	28.0
		401.7	7.2
^{165}Ho(Ne,$\alpha p3n$)^{177}W	2.21 h	115.0	59.0
		185.4[a]	16.1
		376.8	4.6
		416.6	6.1
		1036.9	10.2
^{165}Ho(Ne,$\alpha p4n$)^{176}W	2.50 h	99.4[a]	73.0
^{165}Ho(Ne,$\alpha p6n$)^{174}W	29.00 min	328.3	9.5
		428.6[a]	12.7
^{165}Ho(Ne,$\alpha 2pn$)^{178}Ta^{m}	2.45 h	426.3[a]	97.1
^{165}Ho(Ne,2α)^{177}Ta	56.6 h	112.5[a]	7.2
^{165}Ho(Ne,$2\alpha n$)^{176}Ta	8.10 h	201.7[a]	5.5
		710.5	5.2
^{165}Ho(Ne,$2\alpha 2n$)^{175}Ta	10.50 h	266.1[a]	10.3
		347.7	11.4
^{165}Ho(Ne,$2\alpha 3n$)^{174}Ta	1.18 h	90.9	15.9
		205.7[a]	57.7
^{165}Ho(Ne,$2\alpha 4n$)^{173}Ta	3.65 h	160.4	4.8
		171.5[a]	17.0
^{165}Ho(Ne,$2\alpha p3n$)^{173}Hf	23.60 h	139.6	12.4
		296.5[a]	33.9
^{165}Ho(Ne,$4\alpha 3n$)^{166}Tm	7.70 h	691.2	7.4
		778.4[a]	15.1

[a]γ-lines used for data analysis.

III. ANALYSIS OF FORWARD RECOIL RANGE DISTRIBUTIONS (RRDs) OF THE RESIDUES PRODUCED

The measured cross sections of the reaction products in each foil were divided by the respective foil thickness (in mg/cm^2), to get the normalized yields of various residues produced. The normalized yields [mb/(mg/cm^2)] have been plotted against the cumulative catcher thickness to obtain the differential recoil range distributions. Analysis of the recoil range distribution data of various residues produced in heavy ion induced reactions gives an idea of the linear momentum transfer in the reaction. In the ICF process the linear momentum transferred is proportional to the mass of the projectile fragment fusing with the target nucleus. Thus using RRDs of the residues the relative contribution of ICF in the total fusion cross section has been computed. Owing to partial linear momentum transfer, the forward recoil range in the stopping medium of the residue produced through ICF is expected to be relatively lower than that produced through CF wherein entire linear momentum transfer takes place. Forward recoil ranges of the evaporation residues have also been calculated using the classical approach and the stopping power and range software SRIM [22]. Values of the calculated ranges of the evaporation residues agree well with the measured ones tabulated in Table II.

The measured differential recoil range distributions of 15 evaporation residues produced in the interaction are plotted and displayed in Figs. 3(a)–3(f), 4(a)–4(f), and 5(a)–5(c) and are shown by solid circles. These figures indicate that most of the residues show more than one peak in their RRDs, which are present due to different degrees of linear momentum transfer in incomplete fusion (ICF) of the projectile with the target in addition to the entire linear momentum transfer in complete fusion (CF). In order to compute the relative contributions of complete and incomplete fusion for various evaporation residues the experimentally measured RRD data have been fitted with Gaussian composite peaks using ORIGIN software and are shown by solid curves in Figs. 3–5. The most probable mean range R_P and width parameter (w_A) which is equivalent to standard deviation (σ), has been obtained from the observed recoil range distributions of the various residues and the area under the individual peaks has been computed to obtain the ICF fraction. The peak positions associated with dashed curves in these figures correspond to the entire linear momentum transfer of the projectile ^{20}Ne to the target ^{165}Ho and are obtained at a depth in aluminium catcher foils proportional to the expected recoil range of residues, produced by complete fusion (CF) of the projectile with target. Peak positions associated with dotted curves correspond to

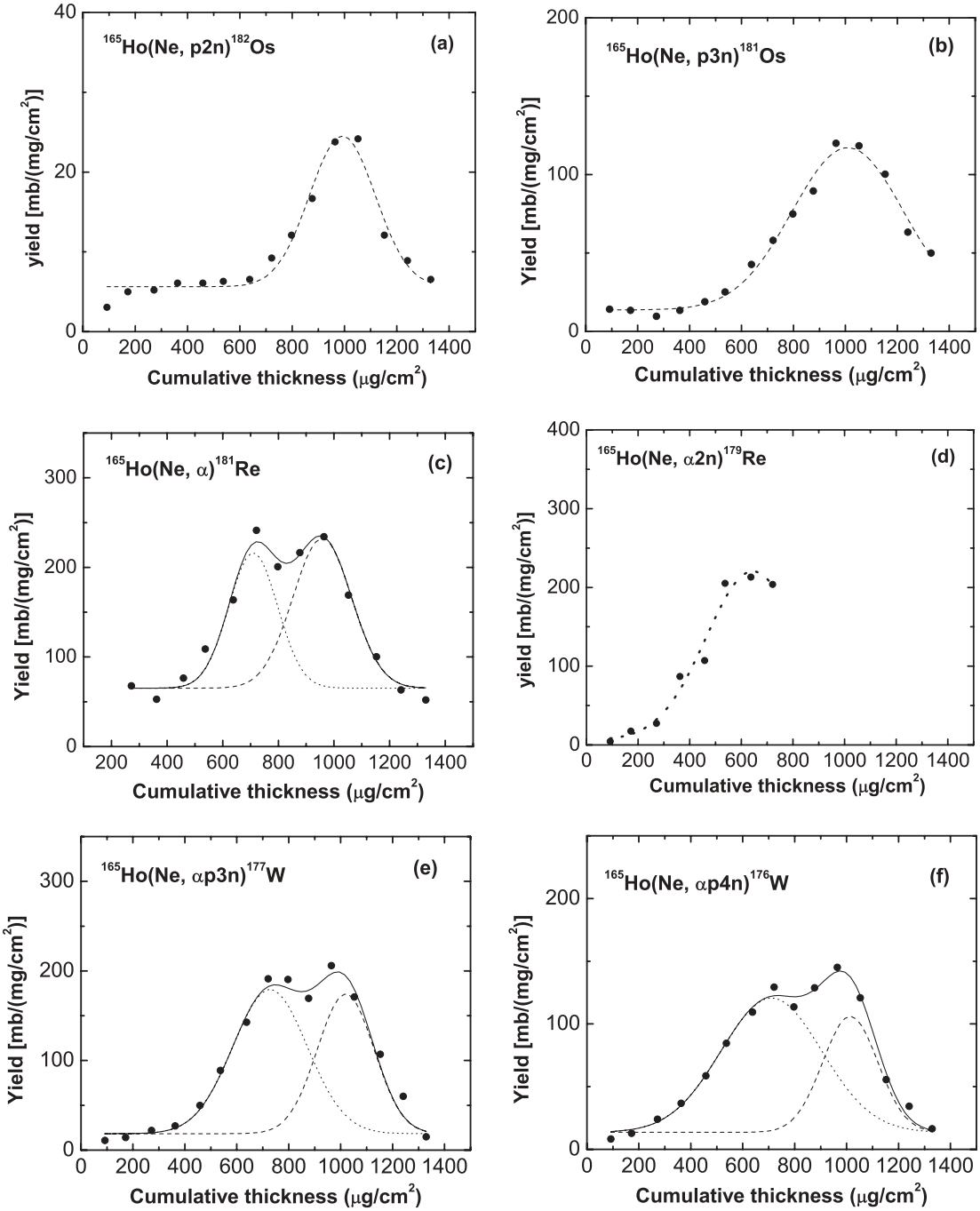

FIG. 3. Gaussian fits to the measured forward recoil range distributions for the evaporation residues ^{182}Os($p2n$), ^{181}Os($p3n$), ^{181}Re(α), ^{179}Re($\alpha 2n$), ^{177}W($\alpha p3n$), and ^{176}W($\alpha p4n$), produced in ^{20}Ne + ^{165}Ho system at ≈164 MeV. Solid circles are the experimental points; dashed curves represent CF of ^{20}Ne; dotted curves represent ICF of ^{20}Ne (fusion of fragment ^{16}O).

the partial momentum transfer of the fragment ^{16}O of the projectile ^{20}Ne to the target and are obtained at the depth in aluminium catcher foils proportional to the expected mean recoil range of residues, produced by incomplete fusion of the fragment ^{16}O with target ^{165}Ho. Similarly, peak positions associated with dot-dashed and dashed-dot-dot curves also correspond to the partial momentum transfer of the fragment ^{12}C and ^{8}Be of the projectile to the target, respectively, and are obtained at the depth in aluminium catcher foils proportional to the expected mean recoil range of residues, produced by incomplete fusion (ICF) of the fragment ^{12}C and ^{8}Be with target ^{165}Ho, respectively. The osmium isotopes, namely ^{182}Os and ^{181}Os, are produced in the reactions ^{165}Ho(Ne, $p2n$)^{182}Os and ^{165}Ho(Ne, $p3n$)^{181}Os, respectively, via complete fusion of ^{20}Ne with ^{165}Ho. The produced compound system ^{185}Ir may decay via the evaporation of one proton and two or three neutrons, respectively, leaving behind the above residues. As can be seen from Figs. 3(a) and 3(b), the observed mean recoil

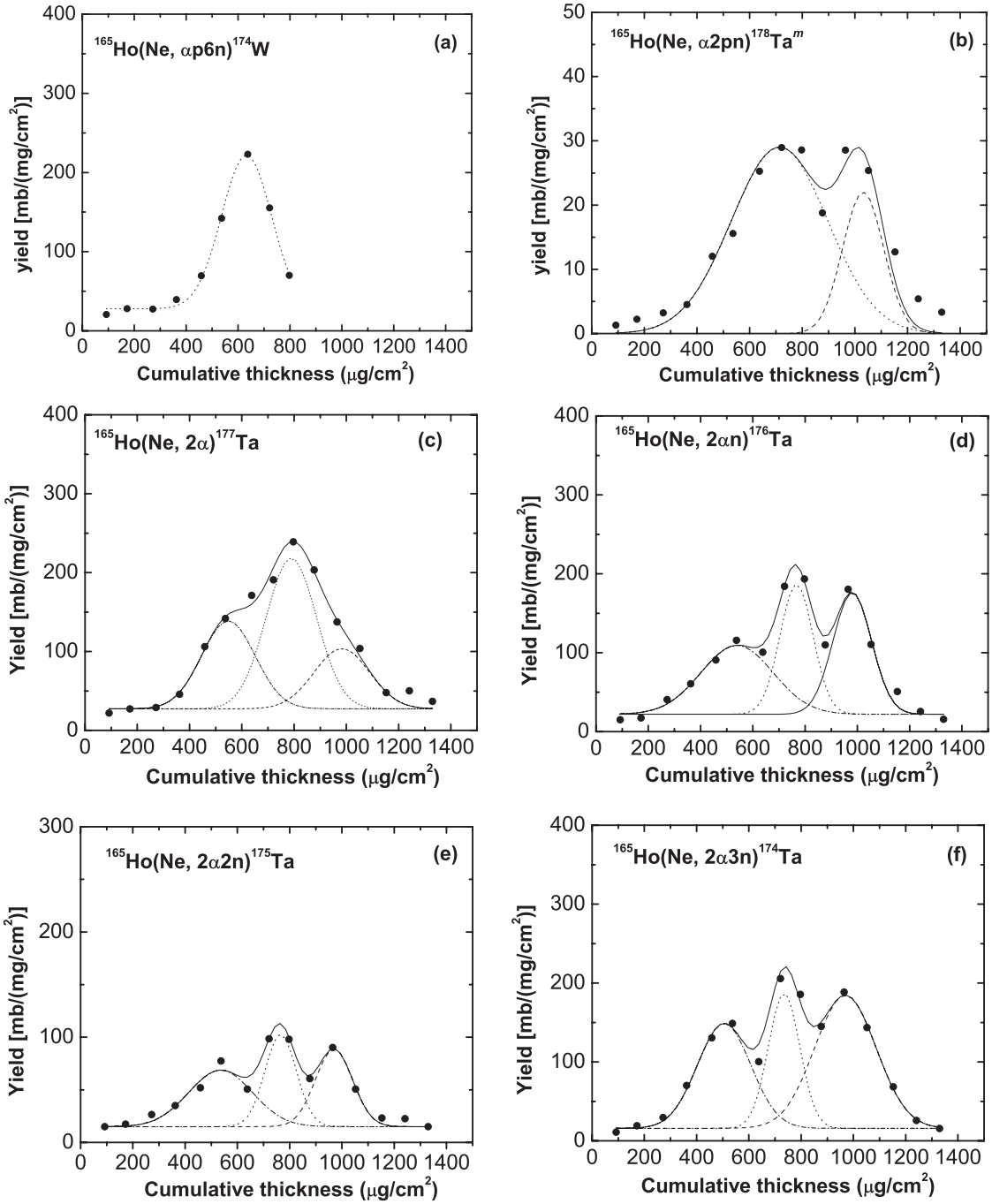

FIG. 4. Gaussian fits to the measured forward recoil range distributions for the evaporation residues ^{174}W($\alpha p6n$), ^{178}Ta^m($\alpha 2pn$), ^{177}Ta(2α), ^{176}Ta($2\alpha n$), ^{175}Ta($2\alpha 2n$), and ^{174}Ta($2\alpha 3n$), produced in ^{20}Ne + ^{165}Ho system at ≈164 MeV. Solid circles are the experimental points; dashed curves represent CF of ^{20}Ne; dotted and dot-dashed curves represent ICF of ^{20}Ne (fusion of fragments ^{16}O and ^{12}C, respectively).

range distributions of residues ^{182}Os and ^{181}Os produced via $p2n$ and $p3n$ emission channels, respectively, show a single peak at cumulative catcher thickness ≈992 and 1009 μg/cm^2 in aluminium, respectively. The observed mean recoil ranges R_p(exp) correspond to the estimated recoil range of the compound system ^{185}Ir, using the classical approach and the stopping power and range software SRIM [22]. It may therefore be inferred that the residues ^{182}Os and ^{181}Os are produced by the complete fusion (CF) process only. The evaporation residue ^{181}Re produced in the reaction ^{165}Ho(^{20}Ne,α)^{181}Re is expected to be populated via complete as well as incomplete fusion of ^{20}Ne with ^{165}Ho. In the case of complete fusion, the compound system ^{185}Ir may decay via the statistical emission of the 1α-particle leaving behind residue ^{181}Re. The same residue may also be populated via incomplete fusion if it is assumed that, as soon as the projectile ^{20}Ne reaches the nuclear

TABLE II. Experimentally measured most probable ranges R_p(exp) of the produced evaporation residues, deduced from RRD curves for CF and ICF components in ^{20}Ne + ^{165}Ho system at ≈164 MeV.

Residues	CF of ^{20}Ne R_p(exp) (μg/cm^2)	ICF of ^{20}Ne		
		Fusion of fragment ^{16}O R_p(exp) (μg/cm^2)	Fusion of fragment ^{12}C R_p(exp) (μg/cm^2)	Fusion of fragment ^{8}Be R_p(exp) (μg/cm^2)
^{182}Os($p2n$)	992 ± 126[a]	–	–	–
^{181}Os($p3n$)	1009 ± 220[a]	–	–	–
^{181}Re(α)	958 ± 99[a]	709 ± 105[a]	–	–
^{179}Re($\alpha 2n$)	–	644 ± 182[a]	–	–
^{177}W($\alpha p3n$)	1019 ± 121[a]	728 ± 151[a]	–	–
^{176}W($\alpha p4n$)	1014 ± 102[a]	710 ± 167[a]	–	–
^{174}W($\alpha p6n$)	–	633 ± 96[a]	–	–
^{178}Ta^m($\alpha 2pn$)	1031 ± 99[a]	709 ± 184[a]	–	–
^{177}Ta(2α)	983 ± 122[a]	789 ± 90[a]	549 ± 92[a]	–
^{176}Ta($2\alpha n$)	980 ± 74[a]	767 ± 62[a]	539 ± 135[a]	–
^{175}Ta($2\alpha 2n$)	970 ± 67[a]	765 ± 62[a]	535 ± 96[a]	–
^{174}Ta($2\alpha 3n$)	973 ± 116[a]	730 ± 62[a]	492 ± 100[a]	–
^{173}Ta($2\alpha 4n$)	1013 ± 147[a]	684 ± 68[a]	438 ± 51[a]	–
^{173}Hf($2\alpha p3n$)	977 ± 58[a]	737 ± 91[a]	451 ± 57[a]	–
^{166}Tm($4\alpha 3n$)	–	721 ± 47[a]	500 ± 46[a]	220 ± 80[a]

[a]Errors are the standard deviations.

field of the target ^{165}Ho, it breaks up into α-clusters viz. ^{4}He and ^{16}O. One of the fragments ^{16}O fuses with the target ^{165}Ho forming an incompletely fused composite system ^{181}Re and the remnant ^{4}He (α-particle) moves in the forward direction. The measured RRD of the evaporation residue ^{181}Re shows two peaks at cumulative catcher thickness ≈958 μg/cm^2 and ≈709 μg/cm^2 in aluminium as shown in Fig. 3(c). Here, the peak at larger cumulative catcher thickness (≈958 μg/cm^2) corresponds to the recoil range of the compound system ^{185}Ir produced via complete fusion of ^{20}Ne with ^{165}Ho, while the peak observed at smaller cumulative catcher thickness (≈709 μg/cm^2) may be produced due to the incomplete fusion of ^{20}Ne (fusion of fragment ^{16}O), because the partial linear momentum transferred is expected to be less than that for the CF of ^{20}Ne with the target ^{165}Ho. This indicates that the reaction ^{165}Ho(^{20}Ne, α)^{181}Re may have contribution not only from CF of ^{20}Ne but also have contribution from ICF of ^{20}Ne (fusion of fragment ^{16}O with ^{165}Ho). The observed mean recoil ranges of residue produced via CF and ICF processes correspond to the theoretically estimated recoil ranges of the compound system ^{185}Ir and composite system ^{181}Re in the stopping medium. Similar observations have been made for other residues and are listed in Table II. The evaporation residue ^{179}Re, produced in the $\alpha 2n$ emission channel may also be populated via CF and ICF processes. However, the measured RRD of this residue as displayed in Fig. 3(d), shows only one peak observed at cumulative catcher thickness ≈644 μg/cm^2, assigned to the mean recoil range of the residues ^{179}Re, produced by the ICF of ^{20}Ne (fusion of fragment ^{16}O with the target ^{165}Ho). It may be pointed out that the recoil range of the same residue

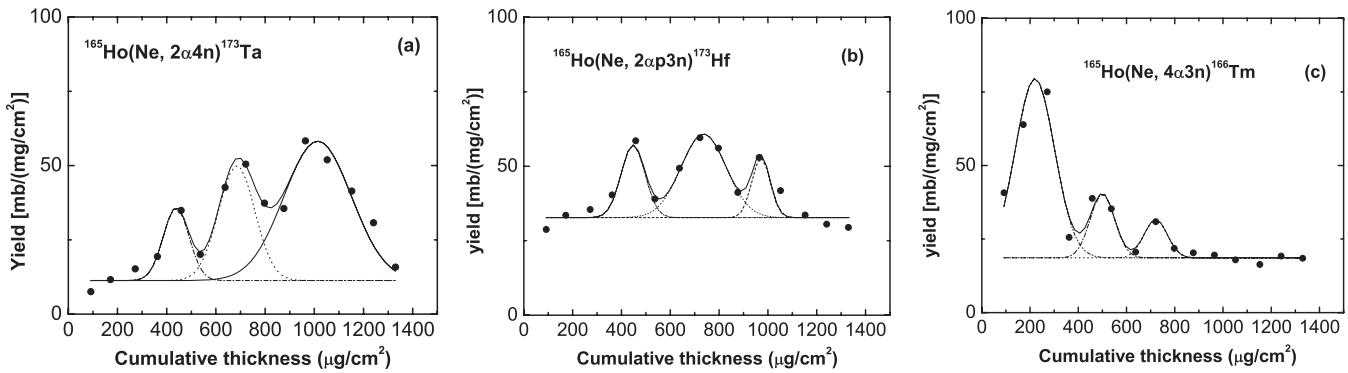

FIG. 5. Gaussian fits to the measured forward recoil range distributions for the evaporation residues ^{173}Ta($2\alpha 4n$), ^{173}Hf($2\alpha p3n$), and ^{166}Tm($4\alpha 3n$), produced in ^{20}Ne + ^{165}Ho system at ≈164 MeV. Solid circles are the experimental points; dashed curves represent CF of ^{20}Ne; dotted, dot-dashed and dashed-dot-dot curves represent ICF of ^{20}Ne (fusion of fragments ^{16}O, ^{12}C, and ^{8}Be, respectively).

TABLE III. Measured relative contributions of CF and ICF at ≈164 MeV ion beam for the system ^{20}Ne + ^{165}Ho.

Reactions	CF of ^{20}Ne	ICF of ^{20}Ne		
		Fusion of fragment ^{16}O	Fusion of fragment ^{12}C	Fusion of fragment ^{8}Be
^{165}Ho(Ne,α)^{181}Re	57%	43%	–	–
^{165}Ho(Ne,$\alpha p3n$)^{177}W	42%	58%	–	–
^{165}Ho(Ne,$\alpha p4n$)^{176}W	32%	68%	–	–
^{165}Ho(Ne,$\alpha 2pn$)^{178}Ta^{m}	24%	76%	–	–
^{165}Ho(Ne,2α)^{177}Ta	21%	49%	30%	
^{165}Ho(Ne,2αn)^{176}Ta	33%	31%	36%	–
^{165}Ho(Ne,2α2n)^{175}Ta	31%	31%	38%	–
^{165}Ho(Ne,2α3n)^{174}Ta	45%	24%	31%	–
^{165}Ho(Ne,2α4n)^{173}Ta	61%	27%	12%	–
^{165}Ho(Ne,2$\alpha p3n$)^{173}Hf	23%	49%	28%	–
^{165}Ho(Ne,4α3n)^{166}Tm	–	9%	17%	74%
Total contribution	35%	44%	19%	2%

^{179}Re produced via the CF process which is expected at a larger range could not be measured due to the order of counting of the catcher foil that has been adopted for the measurement of induced γ-ray activities in this short-lived residue.

The observed forward RRD for the evaporation residue ^{166}Tm produced in the reaction ^{165}Ho(Ne,4α3n)^{166}Tm as shown in Fig. 5(c), there are three resolved peaks corresponding to mean cumulative thickness ≈220, ≈500, and ≈721 μg/cm^2. The observed mean recoil range at cumulative thickness ≈220 μg/cm^2 is due to the ICF of ^{20}Ne with the target ^{165}Ho (where as fusion of fragment ^{8}Be of the projectile ^{20}Ne in the breakup of ^{20}Ne into fragments ^{8}Be and ^{12}C takes place), the observed mean recoil range at cumulative thickness ≈500 μg/cm^2 is due to the ICF of ^{20}Ne with the target ^{165}Ho (whereas the fusion of the fragment ^{12}C produced in the breakup of ^{20}Ne into ^{12}C and ^{8}Be) takes place and the observed mean recoil range peak at cumulative thickness ≈721 μg/cm^2 is due to the ICF of ^{20}Ne (i.e., fusion of fragment ^{16}O in the break-up of ^{20}Ne into ^{16}O and ^{4}He) with the target ^{165}Ho. It is important to note that no peak appears at the cumulative thickness corresponding to the CF process. This shows that this reaction predominantly takes place through various ICF processes. The above descriptions clearly indicate that peaks appearing at different cumulative thicknesses in the stopping medium are related to different degrees of linear momentum transfer from projectile to the target. Experimentally measured most probable ranges R_p(exp) deduced from RRDs via CF and ICF processes for various residues produced are listed in Table II. The relative contributions of the CF and ICF components are obtained by dividing the area of the corresponding peak by the total area under the observed composite RRD curves in Figs. 3(a)–3(f), 4(a)–4(f), and 5(a)–5(c). The relative ICF contributions of the projectile ^{20}Ne (due to the fusion of fragments ^{8}Be, ^{12}C, and ^{16}O) as shown in Fig. 5(c), have been found to be ≈74%, ≈16%, and ≈9%, respectively. As such the relative contributions of the CF and various ICF channels for each residue have been estimated and are listed in Table III. Finally, the total contribution of CF and ICF channels (produced via fusion of projectile fragments ^{16}O, ^{12}C, and ^{8}Be with the target ^{165}Ho) at ≈164 MeV has been evaluated as 35%, 44%, 19%, and 2%, respectively, and is also given in Table III. The overall errors in relative contributions are expected to be less than 15%.

IV. CONCLUSIONS

The forward recoil range distributions (RRDs) of 15 evaporation residues produced in the ^{20}Ne + ^{165}Ho system have been studied at 164 MeV. The measured mean recoil ranges of the residues from the analysis of RRDs strongly reveal a significant contribution from the partial momentum transfer of the projectile associated with incomplete fusion. Different partial linear momentum transfer components are attributed to the fusion of ^{16}O and /or ^{12}C and /or ^{8}Be from the projectile ^{20}Ne to the target nucleus ^{165}Ho. The relative contribution of the components produced via complete and/or incomplete fusion channels in the production of individual residues has been obtained. It has been found that, in general, the residues are not only populated via complete fusion but incomplete fusion also plays an important role in the production of various reaction products involving direct α-cluster emission at the present energy. Present RRD data clearly show that the residues ^{182}Os and ^{181}Os are produced through complete fusion while the residues ^{181}Re, ^{177}W, ^{176}W, ^{174}W, ^{178}Ta, ^{177}Ta, ^{176}Ta, ^{175}Ta, ^{174}Ta,^{173}Ta, and ^{173}Hf are produced via the incomplete fusion channel also. It is also inferred that measurements are consistent with ICF reaction hypothesis of break-up fusion (BUF) wherein fusion of projectile fragments (in its breakup) takes place with the target nucleus. In the measured recoil range distribution of residue ^{166}Tm, the absence of the peak corresponding to the complete fusion channel indicates that the population of this residue predominantly goes through various incomplete fusion channels. A further study of angular distribution of target-like fragments (TLFs) and projectile-like fragments (PLFs) and particle-gamma coincidence studies may provide additional information on incomplete fusion reaction dynamics.

ACKNOWLEDGMENTS

The authors are grateful to Dr. Bikas Sinha, Director, Variable Energy Cyclotron Centre, Kolkata, for providing the experimental facilities to carry out the experiment. The authors are also thankful to Dr. S. K. Basu, Dr. S. K. Saha, and the operational staff of Cyclotron, VECC, Kolkata for providing their good co-operation during the course of this experiment. The authors are also grateful to Dr. B. S. Tomar, Radio-chemistry Division, Bhabha Atomic Research Centre, Mumbai, for valuable discussion and time-to-time help in connection with this study. Travel support provided by Dr. A. K. Sinha, Director, UGC-DAE-Consortium of Scientist Research, Kolkata-Centre, is acknowledged gratefully. The authors are also thankful to the Chairman, Department of Physics, A.M.U, Aligarh, India, for providing the necessary facilities required for this research work.

[1] D. J. Parker, J. Asher, T. W. Conlon, and I. Naqib, Phys. Rev. C **30**, 143 (1984); D. J. Parker, J. J. Hogan, and J. Asher, *ibid.* **35**, 161 (1987).
[2] B. B. Kumar, S. Mukherjee, S. Chakrabarty, B. S. Tomar, A. Goswami, and S. B. Manohar, Phys. Rev. C **57**, 743 (1998).
[3] S. Chakrabarty, B. S. Tomar, A. Goswami, G. K. Gubbi, S. B. Manohar, A. Sharma, B. B. Kumar, and S. Mukherjee, Nucl. Phys. **A678**, 355 (2000).
[4] S. Mukherjee, A. Sharma, S. Sodaye, B. S. Tomar, A. Goswami, and S. B. Manohar, Eur. Phys. J. A **12**, 199 (2001).
[5] M. K. Sharma, Unnati, B. K. Sharma, B. P. Singh, R. Kumar, K. S. Golda, H. D. Bhardwaj, and R. Prasad, Nucl. Phys. **A776**, 83 (2006); M. K. Sharma, Unnati, B. K. Sharma, B. P. Singh, H. D. Bhardwaj, R. Kumar, K. S. Golda, and R. Prasad, Phys. Rev. C **70**, 044606 (2004).
[6] P. P. Singh, M. K. Sharma, Unnati, D. P. Singh, R. Kumar, K. S. Golda, B. P. Singh, and R. Prasad, Eur. Phys. J. A **34**, 29 (2007).
[7] A. Agarwal, I. A. Rizvi, R. Kumar, B. K. Yogi, and A. K. Chaubey, Int. J. Mod. Phys. E **17**, 393 (2008).
[8] P. E. Hodgson, *Nuclear Heavy Ion Reactions* (Clarendon Press, Oxford, 1978).
[9] P. E. Hodgson, E. Gadioli, and E. Gadioli Erba, *Introductory Nuclear Physics* (Oxford University Press, Oxford, 1997).
[10] M. Cavinato *et al.*, in *Heavy Ion Fusion*, edited by A. M. Stefanini *et al.* (World Scientific, Singapore, 1994).
[11] H. C. Britt and A. R. Quinton, Phys. Rev. **124**, 877 (1964).
[12] T. Inamura, M. Ishihara, T. Fakuda, T. Shimoda, and H. Hiruta, Phys. Lett. **B68**, 51 (1977).
[13] P. M. Strudler, I. L. Prešs, and R. Wolfgang, Phys. Rev. **154**, 1126 (1967).
[14] J. Wilczynski, K. Siwek-Wilezynaski, J. Van-Driel, S. Gonggrijp, D. C. J. M. Hageman, R. V. F. Janssens, J. Lukasiak, R. H. Siemssen, and S. Y. Van der Werf, Nucl. Phys. **A373**, 109 (1982).
[15] T. Udagawa and T. Tamura, Phys. Rev. Lett. **45**, 1311 (1980).
[16] M. I. Sobel, P. J. Siemens, J. P. Bondrof, and H. A. Bethe, Nucl. Phys. **A251**, 502 (1975).
[17] J. P. Bondrof, J. N. De, G. Fai, A. O. T. Karvinen, and J. Randrup, Nucl. Phys. **A333**, 285 (1980).
[18] V. Zegrebaev and Y. Penionzhkevich, Prog. Part. Nucl. Phys. **35**, 575 (1995).
[19] D. Singh, M. Afzal Ansari, R. Ali, N. P. M. Sathik, and M. Ismail, J. Phys. Soc. Jpn. **75**, 104201 (2006).
[20] D. Singh, M. Afzal Ansari, R. Ali, N. P. M. Sathik, and M. Ismail, Chin. J. Phys. **46**, 27 (2008).
[21] D. Singh, Ph.D. thesis, Aligarh Muslim University, Aligarh, India (unpublished, 2008).
[22] J. F. Ziegler, SRIM-2006: The Stopping Power and Range of Ions in Matter, 2006.
[23] B. Wilken and T. A. Fritz, Nucl. Instrum. Methods **138**, 331 (1976).
[24] MAESTRO, data acquisition and analysis software coupled with EG & G ORTEC modules (Ridge, USA).
[25] FREEDOM, data acquisition and analysis system designed to support the accelerator based experiments at the Inter University Accelerator Centre, New Delhi, India.
[26] R. B. Firestone and V. S. Shirley, *Table of Isotopes*, 8th ed. (Wiley, New York, 1996).
[27] M. Afzal Ansari, R. K. Y. Singh, M. L. Sehgel, V. K. Mittal, D. K. Avasthi, and I. M. Govil, Ann. Nucl. Energy **11**, 173 (1984).